# Single-cycle versus multicycle nonsequential double ionization of argon

Fang Liu , 1,2,3,\* Zhangjin Chen, Toru Morishita, Klaus Bartschat, Birger Böning, 1,6 and Stephan Fritzsche 1+Helmholtz-Institut Jena, 07743 Jena, Germany

<sup>2</sup>Theoretisch-Physikalisches Institut, Friedrich-Schiller-Universität Jena, 07743 Jena, Germany

<sup>3</sup>Department of Physics, College of Science, Shantou University, 515063 Shantou, Guangdong, China

<sup>4</sup>Institute for Advanced Science, The University of Electro-Communications, 1-5-1 Chofu-ga-oka, 182-8585, Chofu-shi, Tokyo, Japan

<sup>5</sup>Department of Physics and Astronomy, Drake University, Des Moines, Iowa 50311, USA

<sup>6</sup>GSI Helmholtzzentrum für Schwerionenforschung GmbH, 64291 Darmstadt, Germany



(Received 30 April 2021; accepted 28 June 2021; published 9 July 2021)

Using an improved quantitative rescattering model, we calculate the correlated two-electron momentum distributions (CMDs) for nonsequential double ionization of Ar exposed to intense laser pulses with a wavelength of 790 nm at a peak intensity of  $1.0 \times 10^{14}$  W/cm². We analyze the drastic variations in the CMDs that were observed by Kübel *et al.* [New J. Phys. **16**, 033008 (2014)] in the transition from near-single-cycle to multicycle driving laser pulses. Our model reproduces their experimental data well. We also find that the transition from near-single-cycle to multicycle driving laser pulses depends strongly on the details of the pulse envelope. Special attention is paid to the mechanisms responsible for the cross-shaped structure observed experimentally with 4 fs pulses. Our analysis reveals that the cross-shaped structure in the carrier-envelope phase-averaged CMD for near-single-cycle pulses can be attributed to strong backward scattering of the recolliding electron as well as the narrow momentum distributions of the tunnel-ionized electrons compared to those for long pulses. This also explains why the cross-shaped distributions collapse to a rather structureless distribution when the pulse duration is increased to 8 fs.

## DOI: 10.1103/PhysRevA.104.013105

# I. INTRODUCTION

Nonsequential double ionization (NSDI) of atoms in strong laser fields has been studied both theoretically and experimentally, for more than three decades. Experimentally, the total yield of doubly charged ions was first measured as a function of the laser intensity [1–4]. In these experiments, a prominent knee-shaped double-ionization yield was found with increasing intensity. Theoretical predictions based on the *single active electron* approximation, which assumes the sequential emission of independent electrons, differ from the experimental ion yields by many orders of magnitude [2]. It was therefore concluded that the mechanism of nonsequential double ionization must be incorporated to describe the correlated dynamics of two electrons in a strong laser field

Apart from the ion yield, the momentum distributions of doubly and multiply charged ions [5–8] as well as the correlated two-electron momentum distributions (CMDs) [9–14] were reported in the literature. The various measurements provided clear evidence that the emission of the second electron is triggered by the laser-driven recollision of the first electron with its parent ion.

In recent years, due to advances in ultrafast laser technology, CMDs have been measured using few-cycle [15] and near-single-cycle [16] laser pulses with controlled carrier-

envelope phase (CEP). These experiments were able to incorporate only one single recollision event contributing to the NSDI process, thus exploring the ionization dynamics in a single laser cycle. It was found that (i) the CMDs strongly depend on the CEP and (ii) they differ from the CMDs recorded in all previous experiments with many-cycle pulses when averaged over the CEP. In particular, both the so-called *cross-shaped* [16] and *parallel-line* [15] structures in the CMDs were experimentally observed for the first time in few-cycle laser pulses.

The distinct difference of electron correlations between few-cycle and multicycle pulses has further been investigated in measurements for NSDI of Ar exposed to intense laser pulses with a center wavelength of 790 nm and a fixed threshold intensity of  $1.0 \times 10^{14}$  W/cm<sup>2</sup> [17]. Here, the duration of the near transform-limited laser pulses was varied from 4 fs to 30 fs. Interestingly, with 4 fs pulses, a cross-shaped structure was also observed in the CEP-averaged CMD, similar to the experiment performed with 750 nm few-cycle pulses at a much higher peak intensity of  $3.0 \times 10^{14} \text{ W/cm}^2$ [16]. In addition, a major change in the CMDs was found in the few-cycle regime between 4 fs and 8 fs, where the cross-shaped distributions collapse to a rather structureless distribution. As discussed in detail in Ref. [17], this transition from the few-cycle regime to longer pulses is further accompanied by a strong increase in the fraction of anticorrelated to correlated electrons. The experiment was later backed by theoretical studies. In particular, the so-called strongfield approximation (SFA) reproduced the key experimental

<sup>\*</sup>fangfangliu2020@gmail.com

findings by choosing appropriate coherent superpositions of excitation channels [18].

The cross-shaped CMDs measured with near-single-cycle short pulses are of special interest since this cross-shaped structure has never been observed for long pulses. Various theoretical models have been used to investigate its observation at high intensity [16,19–22]. The debate on the physical mechanism responsible for this structure was effectively settled by a recent study using the quantitative rescattering (QRS) model [23] that is based on the factorization formula in [24,25]. Until now, however, the mechanism for the crossed-shaped structure observed in the latter experiment with a lower intensity [17] has been studied much less, and the collapse of this structure in the CMD for few-cycle pulses has eluded a satisfying theoretical explanation [18]. On the one hand, calculations based on the so-called three-dimensional classical ensemble model indicated that recollision-induced excited states are ionized in the strong laser field for a duration much longer than one optical cycle [26]. While this can lead to differences in the observed CMDs for few-cycle and multicycle pulses, it is commonly believed that these excited states should be ionized within one optical cycle [6,16]. Therefore, the details of the ionization mechanism and the relationship between the pulse duration and anticorrelations in the CMD still remain to be understood.

In this paper, we use a recently improved QRS model [27] to compute the CMDs measured in the experiments for NSDI of Ar performed by Kübel et al. [17] and focus on the transition from the near-single to the multicycle regime. As will be explained below, the cross-shaped structure in the CEP-averaged CMD observed in this experiment can be attributed to strong backward scattering of the recolliding electron as well as the temporal shape of the few-cycle pulse. This explanation is very different from that suggested by Chen et al. [23] for the generation of the cross-shaped structure first observed at high intensity [16]. The single-cycle and multicycle CMDs measured in the experiment [17] are both well reproduced by the QRS model, and the transition from the near-single-cycle to the multicycle regime is due to the changing temporal shape of the laser pulses. The resulting theoretical understanding shall not only lead to a quantitative explanation of the above-mentioned experiment, but will also enhance the understanding of the underlying NSDI dynamics in general.

This paper is structured as follows. In Sec. II, we introduce the theoretical method used to calculate the CMDs for NSDI within the QRS model. We then show our theoretical results in Sec. III. Furthermore, we shall compare our results with the experimental data and discuss the theoretical results. Finally, we present our conclusions and give an outlook for future work in Sec. IV.

Unless indicated otherwise, atomic units ( $m_e = e = \hbar = 4\pi \varepsilon_0 = 1$ ) are used throughout the manuscript.

# II. THEORETICAL MODEL

We aim to calculate the CMDs for NSDI of Ar illuminated by an intense laser beam. Upon interaction with the beam, the atom is doubly ionized and two electrons are emitted with momenta  $p_1$  and  $p_2$ , which are simultaneously measured at two detectors. The CMDs are the momentum distributions of the two outgoing electrons along the linear polarization direction of the laser field.

The underlying physics of NSDI can been understood in terms of the classical rescattering model [28] in the following way: a first electron, liberated via tunnel ionization, is accelerated by the laser field in the continuum and driven back to the parent ion. It may then recollide with the parent ion, leading to a second electron being ionized through recollision direct ionization (RDI) or recollision excitation with subsequent ionization (RESI). Essential to this rescattering picture is that there exists a laser-induced recolliding wave packet (RWP) (the first electron), which can initiate collisions with the ionic core. However, because this RWP exists only in the laser field, it cannot be measured directly.

While laser-induced rescattering processes can be qualitatively interpreted by the classical rescattering model, the QRS model provides a quantitative description. The QRS model was first proposed for high-order above-threshold ionization (HATI) due to elastic scattering of the returning electron from the parent ion [29], in which the RWP is extracted from the two-dimensional (2D) momentum distributions for HATI photoelectrons calculated using the SFA [30]. Since all the rescattering processes are induced by the same RWP, the RWP obtained for HATI can be used for NSDI. For this purpose, we first briefly review the SFA model for single ionization.

#### A. Strong-field approximation

In the familiar SFA for single ionization, the first two terms of the perturbation series, called SFA1 and SFA2, respectively, express the momentum-dependent ionization amplitude as [30,31]

$$f_{SFA}(\mathbf{p}) = f_{SFA1}(\mathbf{p}) + f_{SFA2}(\mathbf{p}), \tag{1}$$

where p is the momentum of the detected photoelectron. The direct ionization amplitude in Eq. (1) is given by

$$f_{\text{SFA1}}(\boldsymbol{p}) = -i \int_{-\infty}^{\infty} dt \left\langle \chi_{\boldsymbol{p}}(t) | \boldsymbol{r} \cdot \boldsymbol{F}(t) | \Psi_{i}(t) \right\rangle, \qquad (2)$$

where F(t) is the laser electric field that is linearly polarized along the z axis,

$$\mathbf{F}(t) = \cos^2\left(\frac{\pi t}{\tau}\right) F_0 \cos(\omega t + \phi) \hat{\mathbf{z}},\tag{3}$$

with the carrier frequency  $\omega$  and the CEP  $\phi$  for the time interval  $(-\tau/2, \tau/2)$  and zero elsewhere. The pulse duration, defined as the full width at half maximum (FWHM), is given by  $\Gamma = \tau/2.75$ . In Eq. (2),  $\Psi_i(t)$  is the initial ground-state wave function and  $\chi_p$  is a so-called Volkov state given by

$$\langle \mathbf{r} | \chi_{\mathbf{p}}(t) \rangle = \frac{1}{(2\pi)^{3/2}} e^{i[\mathbf{p} + \mathbf{A}(t)] \cdot \mathbf{r}} e^{-iS(\mathbf{p}, t)}, \tag{4}$$

where A(t) is the vector potential and the action S is

$$S(\boldsymbol{p},t) = \frac{1}{2} \int_{-\infty}^{t} dt' [\boldsymbol{p} + \boldsymbol{A}(t')]^{2}.$$
 (5)

The second term in Eq. (1), called SFA2, accounts for laser-induced elastic scattering of the returning electron from the

parent ion. This rescattering amplitude can be expressed as

$$f_{SFA2}(\mathbf{p}) = -\int_{-\infty}^{\infty} dt \int_{t}^{\infty} dt' \int d\mathbf{k} \langle \chi_{\mathbf{p}}(t') | V | \chi_{\mathbf{k}}(t') \rangle \times \langle \chi_{\mathbf{k}}(t) | \mathbf{r} \cdot \mathbf{F}(t) | \Psi_{i}(t) \rangle,$$
(6)

where V is the scattering potential. It takes the form

$$V(r) = \widetilde{V}(r)e^{-\alpha r},\tag{7}$$

where  $\alpha$  is a screening factor introduced to avoid the singularity in the integrand in Eq. (6) and  $\widetilde{V}(r)$  is the atomic model potential given by

$$\widetilde{V}(r) = -\frac{1 + a_1 e^{-a_2 r} + a_3 r e^{-a_4 r} + a_5 e^{-a_6 r}}{r}.$$
 (8)

The parameters  $a_i$  in Eq. (8) for Ar can be found in Ref. [32]. Clearly, the rescattering amplitude consists of three time-ordered steps by the electron: tunnel ionization, propagation in the laser field, and elastic scattering with the parent ion.

### B. Recolliding wave packet

According to the QRS model, the momentum distribution of the HATI photoelectron with momentum p can be expressed as a product of the momentum distribution of the RWP and the differential cross section (DCS) for elastic scattering of the returning electron from the parent ion [29]. By defining the HATI photoelectron momentum distribution obtained from the SFA as

$$D_{\text{SFA2}}^{\text{HATI}}(\boldsymbol{p}) = |f_{\text{SFA2}}(\boldsymbol{p})|^2, \tag{9}$$

the QRS model for HATI reads

$$D_{\text{SFA2}}^{\text{HATI}}(\mathbf{p}) = W(k_r) \frac{d\sigma_{\text{PWBA}}^{\text{el}}(k_r, \theta_r)}{d\Omega_r}, \tag{10}$$

where  $W(k_r)$  is the RWP describing the momentum distribution of the returning electron with kinetic energy  $E_r = k_r^2/2$ , and  $d\sigma_{\text{PWBA}}^{\text{el}}(k_r, \theta_r)/d\Omega_r$  is the DCS, calculated within the plane-wave first-order Born approximation (PWBA), for an electron with a momentum of magnitude  $k_r$  scattered at an angle  $\theta_r$  with respect to the direction of the returning electron. The detected photoelectron momentum p and the momentum  $k_r$  of the scattered electron are related by [29]

$$p = k_r - A_r, \tag{11}$$

with

$$k_r = 1.26|A_r|,$$
 (12)

where  $A_r \equiv A(t_r)$  is the vector potential at the recollision time  $t_r$ . The relation between  $k_r$  and  $|A_r|$  is determined approximately by solving Newton's equation of motion for an electron in a monochromatic laser field, which yields the factor 1.26 derived in Ref. [29].

With the HATI photoelectron momentum distribution calculated using SFA2 and the DCS for elastic scattering of the returning electron with the parent ion evaluated using PWBA, the momentum distribution of the RWP is obtained by Eq. (10). It is worth mentioning that this momentum distribution does not depend on the rescattering angle  $\theta_r$  and can therefore be calculated at an arbitrary angle. In practice, a large scattering angle, around  $\theta_r = 178^{\circ}$ , is usually chosen.

### C. QRS model for NSDI

As mentioned above, the generally accepted mechanisms for NSDI are RDI and RESI [6]. However, according to the classical rescattering model, the maximum energy of the laser-induced returning electron, in the experiments [17] considered here, is about 18.5 eV, which is much less than the ionization potential of Ar<sup>+</sup> (27.2 eV). Consequently, RDI can be ruled out, and we only consider RESI in the present work. Since the details of the improved QRS model for RESI have been presented in Refs. [27,33], only a brief summary is given here.

By applying the philosophy of the QRS model for HATI to NSDI, the CMD  $D(p_{\parallel}^1,p_{\parallel}^2)$  for RESI can be factorized as a product of the energy distributions of the RWP and the parallel momentum distributions  $D_{E_i,I}^{(\text{RESI})}(p_{\parallel}^1,p_{\parallel}^2)$  of the two outgoing electrons [34,35]. This yields

$$D(p_{\parallel}^{1}, p_{\parallel}^{2}) = \int_{l_{p}^{(\text{exc})}}^{\infty} dE_{i} D_{E_{i}, I}^{(\text{RESI})}(p_{\parallel}^{1}, p_{\parallel}^{2}) W_{I}(E_{r}), \qquad (13)$$

where  $I_p^{(\mathrm{exc})}$  is the threshold energy for excitation and  $W_I(E_r)$  is the RWP describing the energy distribution of the returning electron in the laser field at a single intensity I. In Eq. (13) an integral over  $E_i$  is performed to account for the contributions from collisions at all incident energies. At a single peak intensity (i.e., without focal-volume averaging, which we assume in this manuscript unless specified otherwise), the CMD of the two outgoing electrons in RESI can further be expressed as a product of the parallel momentum distribution  $D_{E_i,I}^{(\mathrm{exc})}(p_\parallel^1)$  of the first rescattered electron after recollisional excitation and the parallel momentum distribution  $D_I^{(\mathrm{tun})}(p_\parallel^2)$  of the second electron that is tunnel ionized from the excited state, i.e.,

$$D_{E_{i},I}^{(\text{RESI})}(p_{\parallel}^{1}, p_{\parallel}^{2}) = D_{E_{i},I}^{(\text{exc})}(p_{\parallel}^{1}) \times D_{I}^{(\text{tun})}(p_{\parallel}^{2}). \tag{14}$$

The first rescattered electron is described by the DCSs for electron impact excitation of  $Ar^+$  that are calculated with the nonperturbative close coupling with pseudostates method using a fully parallelized B-spline R-matrix code [36,37]. Experimentally, the CMDs are only measured for the momentum components of the two electrons along the laser polarization axis. Thus, to compare with experiment, the DCS  $d\sigma_{\rm exc}/d\Omega$  for laser-free electron impact excitation of the parent ion needs to be projected onto the polarization direction. Since the DCS is symmetric around the incident direction, the parallel momentum distribution of the scattered electron at incident energy  $E_i$  is given by

$$Y_{E_i}^{(\text{exc})}(k_{\parallel}^1) = \frac{2\pi}{k^1} \frac{d\sigma_{\text{exc}}(\theta)}{d\Omega},\tag{15}$$

where  $k^1$  is the momentum of the projectile electron after collision and  $k_{\parallel}^1 = k^1 \cos \theta$ , with  $\theta$  being the scattering angle. For laser-induced recollision excitation, the scattered electron is still under the influence of the laser field after the collision, such that it will gain an additional momentum  $A_r$  in the direction of the laser polarization from the recollision time  $t_r$  to the end of the laser pulse. Hence the parallel momentum distribution of the recollisional excitation process at an intensity I can be obtained from Eq. (15) by shifting the momentum of the first rescattered electron by  $A_r$ , i.e.,

$$D_{E_i,I}^{(\text{exc})}(p_{\parallel}^1) = Y_{E_i}^{(\text{exc})}(k_{\parallel}^1 - A_r). \tag{16}$$

In the improved QRS model for NSDI, the lowering of the threshold due to the presence of the electric field at the instant of recollision is taken into account [27]. It was argued by van der Hart and Burnett [38] that, in contrast to the collisions taking place in a field-free environment, the threshold energy for the laser-induced inelastic collision of the returning electron with the parent ion could be lowered by

$$\Delta E = 2\sqrt{Z_{\text{eff}}|F_r|},\tag{17}$$

where  $F_r$  is the electric field at the instant of collision. For electron impact excitation and ionization of a singly charged ion,  $Z_{\rm eff}=1$  and 2, respectively. To account for the lowering of the threshold energy, the collision energy should be adjusted to

$$E_r = E_i - \Delta E, \tag{18}$$

where  $E_i$  is the incoming electron energy in the field-free case. Correspondingly, Eq. (12) should be rewritten as

$$|A_r| = \sqrt{2(E_i - \Delta E)}/1.26.$$
 (19)

The process of tunneling ionization from the excited state of  $Ar^+$  is described by solving the time-dependent Schrödinger equation (TDSE) within the single-active-electron approximation [25,39]. By integrating the 2D momentum distribution, evaluated by solving the TDSE for single ionization of electrons from excited  $Ar^+$ , over the momentum components perpendicular to the laser polarization, we obtain the parallel momentum distribution  $D_I^{(\text{tun})}(p_\parallel^2)$  of the second electron.

With the prepared parallel momentum distribution of the first returning electron after recollision and the parallel momentum distribution of the second electron tunnel-ionized from an excited state of the parent ion, respectively, the CMD for laser-induced electron impact excitation at incident energy  $E_i$  with subsequent tunneling ionization in the laser field with a peak intensity I can be obtained by Eq. (14) and the CMD for RESI at a single peak intensity can be evaluated by performing the integral over the impact energy in Eq. (13).

# III. RESULTS AND DISCUSSION

On the basis of the theory outlined in the previous section, we simulate the CMDs for NSDI of Ar in both the near-single-cycle as well as the multicycle regime, and investigate the variations in the shapes of the CMD accompanied by a change in laser pulse duration. In doing so, we will be guided by the experiment [17]. As already discussed above, for the experimental conditions considered here, only the RESI process contributes to the NSDI of Ar.

## A. Scattering cross sections for electron impact excitation

We present in Figs. 1(a)-1(c) the DCSs for laser-free electron impact excitation of  $Ar^+$  from the  $(3s^23p^5)$  ground state to the excited states  $3s3p^6$ ,  $3s^23p^43d$ , and  $3s^23p^44s$  at incident energies of 17, 20, 23, and 25 eV, respectively. These DCSs can be used to simulate the parallel momentum distributions of the first electron after recollision excitation in the laser fields with different laser parameters, in particular, the pulse duration. Both the magnitude and structure of the DCSs

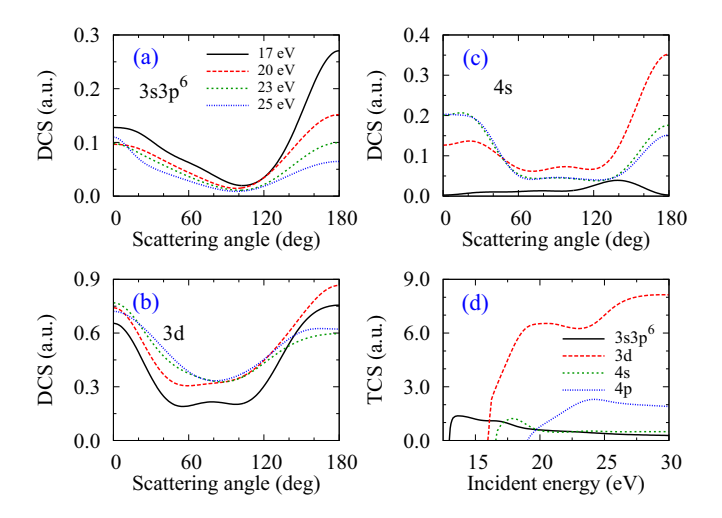


FIG. 1. Angle-differential cross sections  $d\sigma_{\rm exc}/d\Omega$  for electron impact excitation of Ar<sup>+</sup> from the ground state to (a)  $3s3p^6$ , (b)  $3s^23p^43d$ , and (c)  $3s^23p^44s$  configurations at incident energies of 17 eV, 20 eV, 23 eV, and 25 eV, respectively. In panel (d), the total cross sections (TCS) for electron impact excitation of Ar<sup>+</sup> to the excited states  $3s3p^6$ ,  $3s^23p^43d$ ,  $3s^23p^44s$ , and  $3s^23p^44p$  are displayed.

play an important role in forming the CMDs. The DCSs for  $3s^23p^43d$  are about three times larger than those for  $3s3p^6$  and  $3s^23p^44s$ . All the DCSs exhibit strong backward scattering for the energies considered here. The dominant excitation to  $3s^23p^43d$  [cf. Fig. 1(d)] is a result of the large overlap of the 3p and 3d orbitals in the radial coordinates. On the other hand, the total cross section for excitation to  $3s^23p^44p$  is much smaller than that for  $3s^23p^43d$  at collision energies below 20 eV. Thus excitations to  $3s^23p^44p$  and even higher excited states can be safely neglected in the calculations of CMDs for NSDI of Ar under the experimental conditions considered here.

# B. Cross-shaped CMD for a pulse duration of 4 fs

We first focus on the CMDs for RESI of Ar in 790 nm and 4 fs laser pulses with a peak intensity of  $1.0 \times 10^{14}$  W/cm². To compare with the CEP-averaged CMD measured by Kübel *et al.* [17], we calculate the CMDs for  $\phi$  ranging from 0° to 150° in steps of 30°. For each CEP, we evaluate the parallel momentum distributions of the two outgoing electrons and the momentum distributions of the RWP for the laser-induced returning electron.

The parallel momentum distributions of the first rescattered electron after recollision are obtained by projecting the DCSs for laser-free electron impact excitation of  $Ar^+$  onto the polarization direction with the parallel momentum shifted by  $-A_r$ . For a selected CEP value of  $60^\circ$ , the results are displayed in Figs. 2(a)-2(c) for excitation of the residual ground-state electron to the excited states  $3s3p^6$ ,  $3s^23p^43d$ , and  $3s^23p^44s$  of  $Ar^+$  at energies of 17 eV, 20 eV, and 23 eV for the situation in which the laser-induced electron returns to the parent ion along  $-\hat{z}$ , i.e., the negative beam polarization direction. The smallest and largest parallel momenta correspond to the scattering angles of  $\theta_r = 0^\circ$  and  $\theta_r = 180^\circ$  with respect to the

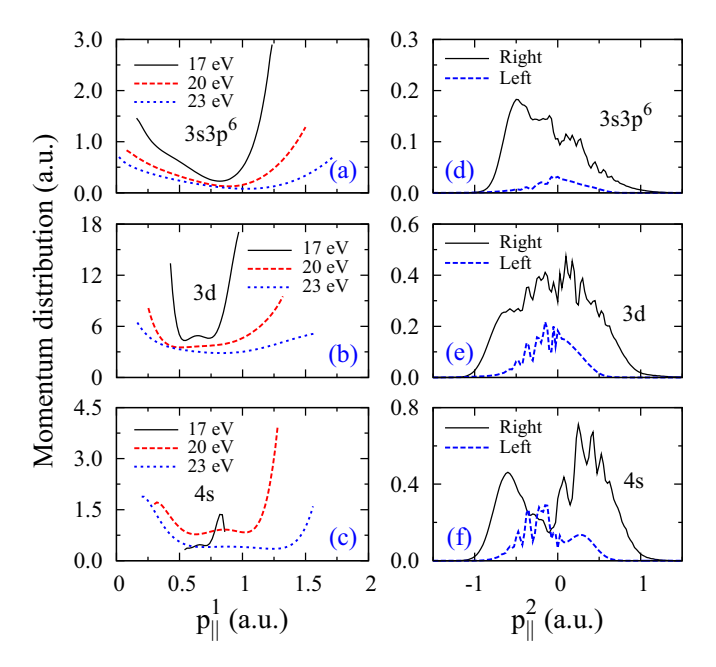


FIG. 2. Parallel momentum distributions  $D_{E_i,I}^{(\rm exc)}(p_{\parallel}^1)$  (left column) and  $D_I^{(\rm tun)}(p_{\parallel}^2)$  (right column) of two outgoing electrons in RESI of Ar by a 790 nm, 4 fs laser pulse with a peak intensity of  $1.0 \times 10^{14}$  W/cm² and a CEP of 60°. Results are shown for the first returning electron after recolliding with the Ar+ ion and exciting the residual ground-state electron to the excited states  $3s3p^6$  (a),  $3s^23p^43d$  (b), and 4s (c) at energies of 17 eV, 20 eV, and 23 eV for the situation in which the laser-induced electron returns to the parent ion along the  $-\hat{z}$  direction, and for the tunneling electron escaping from Ar+ in the excited states  $3s3p^6$  (d),  $3s^23p^43d$  (e), and  $3s^23p^44s$  (f).

direction of the returning electron. As expected, the momentum distributions imprint the behavior of the DCSs shown in Fig. 1. Due to the strong backward scattering, the parallel momentum distributions of the first rescattered electron at large momenta are comparable to those at small momenta.

Figures 2(d)–2(f) display the parallel momentum distributions of the second excited tunnel electron as obtained by solving the TDSE for a CEP  $\phi = 60^{\circ}$ . The notations right and left used here refer to the situations in which the first rescattered electron returns to the parent ion along the negative and positive  $\hat{z}$  directions, respectively. The results show that the right-side parallel momentum distributions are higher and wider than those for the left side. This is due to the fact that, with respect to the right side, the initial tunnel-ionization time for the left side is half a cycle later for  $\phi = 60^{\circ}$  (see Fig. 3 in Ref. [23]). Consequently, the instantaneous fields under which the second electron is tunnel ionized are much weaker owing to the rapid decrease of the envelope for such a short pulse. The difference between the left and right distributions also exists as the CEP changes, but the ratio of the total ionization yields between the left and right distributions varies. On the other hand, it should be noted that the parallel momentum distributions for the left and right sides are almost identical for long pulses.

Next, we present the momentum distributions of the RWP that account for the weight of contributions from recollisions

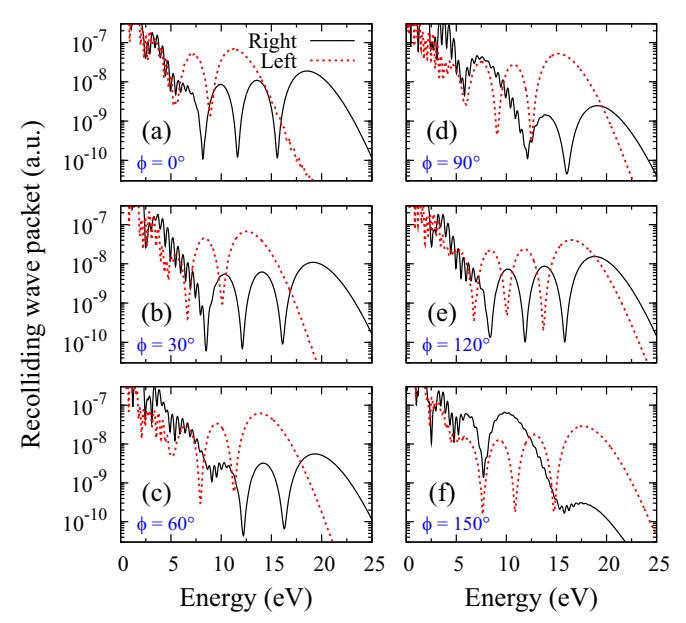


FIG. 3. Energy distribution of the recolliding wave packet  $W_I(E_r)$  for the first returning electron computed from SFA2 for single ionization of Ar by 790 nm, 4 fs laser pulses at a peak intensity of  $1.0 \times 10^{14} \text{ W/cm}^2$  with CEPs of (a)  $0^{\circ}$ , (b)  $30^{\circ}$ , (c)  $60^{\circ}$ , (d)  $90^{\circ}$ , (e)  $120^{\circ}$ , and (f)  $150^{\circ}$ , respectively.

at all possible energies. The RWPs are extracted from the 2D momentum distributions for HATI of Ar. For short laser pulses with a duration of 4 fs, the RWP is highly CEP dependent, and the right-side and left-side RWPs for a fixed CEP are significantly different. In contrast to the situation of long pulses in which the 2D momentum distributions for HATI are almost left-right symmetric along the  $\hat{z}$  direction, for short pulses we should distinguish the returns of the first rescattered electron to the target ion from different directions. The right-side and the left-side RWPs for electrons returning along the negative and positive  $\hat{z}$  directions, respectively, are calculated for 790 nm, 4 fs laser pulses with peak intensity of  $1.0 \times 10^{14} \text{ W/cm}^2$  within the SFA2, and the results for CEPs ranging from  $0^{\circ}$  to  $150^{\circ}$  with a step size of  $30^{\circ}$  are shown in Fig. 3. Generally, each RWP decreases dramatically at low energies with increasing energy, followed by a plateau in the high-energy region with oscillations until a cutoff is reached. The left-side RWP becomes weaker and extends to higher energies as the CEP increases, while the trend reverses for the right-side RWP. Note that, for CEPs from 180° to 360°, the roles of left and right RWPs are interchanged.

With all the above ingredients carefully prepared, the calculation of CMD for RESI is straightforward by performing the integration in Eq. (13), in which the contributions from recollisions at all incident energies are considered. Here, the change of the threshold energy due to the presence of the electric field at the instant of recollision is taken into account as well. As expected, the calculated CMDs demonstrate that excitation to  $3s^23p^43d$  dominates. Hence we only present the results for  $3s^23p^43d$  here. The left- and right-side CMDs for recollision excitation of  $Ar^+$  to  $3s^23p^43d$  with subsequent ionization in a 790 nm, 4 fs laser pulse with a peak intensity of  $1.0 \times 10^{14}$  W/cm² and a CEP of  $\phi = 60^{\circ}$  are displayed

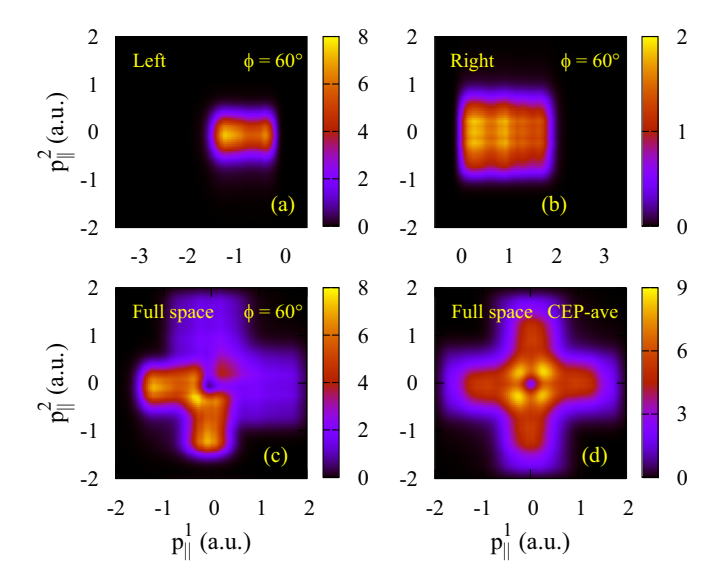


FIG. 4. Correlated two-electron momentum distribution  $D(p_{\parallel}^1,p_{\parallel}^2)$  following RESI in NSDI of Ar in 790 nm, 4 fs laser pulses at a peak intensity of  $1.0\times 10^{14}$  W/cm² for the tunneling electron ionized from Ar<sup>+</sup>(3s²3p⁴3d).  $p_{\parallel}^1$  and  $p_{\parallel}^2$  denote the photoelectron momenta along the laser polarization. Distributions are shown for a CEP of  $\phi=60^{\circ}$  in panels (a)–(c) and CEP averaged in (d). See text for details.

in Figs. 4(a) and 4(b), respectively. In the left-side CMD the electron pairs cluster in a smaller region with larger magnitude compared to the right-side CMD. The difference in magnitude between the right-side and left-side CMDs is attributed to the difference in magnitude between the right-side and leftside RWPs, as shown in Fig. 3(c). Furthermore, the cutoff energy in the left-side RWP is smaller than that in the right-side one. Hence the contributions to the left-side CMD originate from recollisions at lower impact energies with more pronounced backward scattering, leading to a slightly narrower distribution along  $p_{\parallel}^1$  with higher density at large momenta (absolute value of  $p_{\parallel}^1$ ) in the left-side CMD than in the right-side one. In addition, while the right-side CMD exhibits an almost squarelike structure, the distribution along  $p_{\parallel}^2$  on the left-side CMD is more compact. This directly reflects the difference in the width between the left-side and right-side parallel momentum distributions for the second tunnel-ionized electron, as displayed in Fig. 2(e).

Since the two electrons emitted in NSDI are indistinguishable, the CMD for excitation tunneling should be symmetric with respect to the diagonal  $p_{\parallel}^1=p_{\parallel}^2$ . Figure 4(c) depicts the full-space CMD when the CMDs displayed in Figs. 4(a) and 4(b) are symmetrized. Since the magnitude of the left-side CMD in Fig. 4(a) is about four times larger than the right side in Fig. 4(b), in the symmetrized CMD the distributions below the diagonal  $p_{\parallel}^1=-p_{\parallel}^2$  dominate.

In Fig. 4(d) we depict the CEP-averaged CMD for excitation tunneling from the excited state  $3s^23p^43d$ . Owing to the pronounced arms shown in Fig. 4(a), the CEP-averaged CMD exhibits a cross-shaped structure. As discussed above, the side arms of the cross-shaped structure are formed as a result of the relatively uniform distribution of the signals on the  $p_{\parallel}^1$  axis due to the strong backward scattering of the first electron and

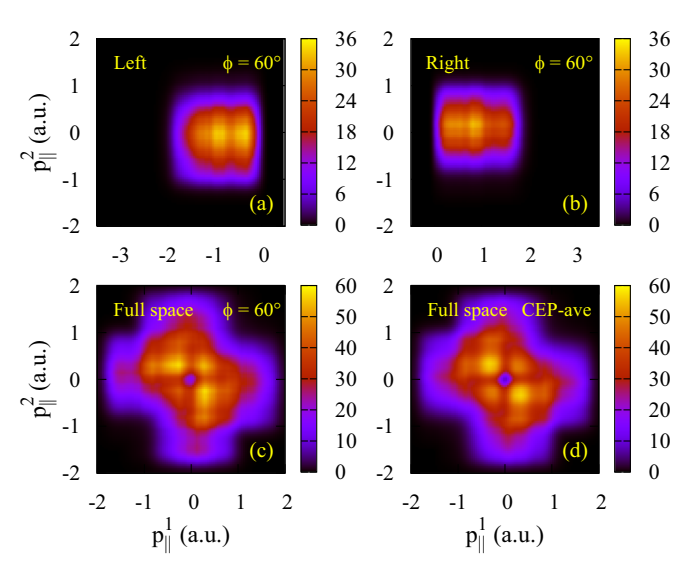


FIG. 5. Same as Fig. 4 for a pulse duration of 8 fs.

the narrow distribution peaked around zero on the  $p_{\parallel}^2$  axis for reasons that will be discussed below.

It should be noted that, in contrast, the cross-shaped structure in the CMD for NSDI of Ar observed in an earlier experiment [16] at a higher peak intensity of  $3.0 \times 10^{14} \ \text{W/cm}^2$  was ascribed to the strong *forward* scattering of the recolliding electron as well as the depletion effect in tunneling ionization of the second electron [23]. This is due to the fact that, at  $3.0 \times 10^{14} \ \text{W/cm}^2$ , the maximum energy of the returning electron increases to about 50 eV. Then forward scattering prevails, leading to sharp distributions at small momenta (absolute value) on the  $p_{\parallel}^1$  axis. Consequently, the cross-shaped structure for the high intensity is formed as a result of the *leg* rather than the *arm* for the low intensity.

### C. Collapse of the cross shape in the CMD for 8 fs

As demonstrated by the measurements [17], the characteristic cross-shaped structure in the CMD for 4 fs collapses when the pulse duration is increased to 8 fs. This sudden change in the observed CMDs is confirmed by our theoretical simulations. In Fig. 5, we show the calculated CMD for RESI in NSDI of Ar in 790 nm, 8 fs laser pulses at a peak intensity of  $1.0 \times 10^{14} \text{ W/cm}^2$  for the tunneling electron ionized from  $Ar^+(3s^23p^43d)$ . One can see from Figs. 5(a) and 5(b) that, when the pulse duration increases to 8 fs, only slight differences exist between the left-side and right-side CMDs in both magnitude and shape, indicating that the CEP dependence of the CMD becomes weak. Furthermore, the striking resemblance between the symmetrized full-space CMD for a given CEP in Fig. 5(c) and the CEP-averaged one in Fig. 5(d) confirms again the weak CEP dependence of the CMDs for 8 fs. Clearly, the structure of the CEP-averaged CMD for a pulse duration of 8 fs is qualitatively different from that for 4 fs. This remarkable discrepancy is certainly a direct result of the increase of pulse duration.

A detailed understanding of the sudden change in the NSDI dynamics accompanying the transition into the fewcycle regime can be gained from a close look at the

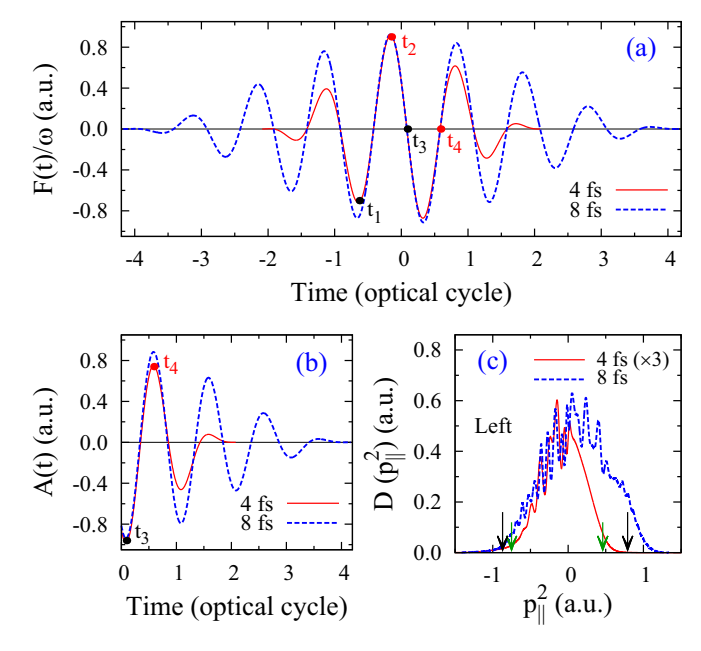


FIG. 6. (a) Electric fields and (b) vector potentials ( $t \ge 0$ ) for laser pulses with pulse durations of 4 fs (red solid curves) and 8 fs (blue dashed curves), respectively, with peak intensity  $I=1.0\times 10^{14}~\rm W/cm^2$ , wavelength  $\lambda=790~\rm nm$ , and CEP  $\phi=60^\circ$ . (c) Parallel momentum distributions of the second tunneling electron escaping from Ar<sup>+</sup> in  $3s^23p^43d$  calculated by solving the TDSE for the situation in which the first rescattered electron returns to the parent ion along the  $+\hat{z}$  direction. The short and long arrows indicate the upper limits, obtained based on the one-dimensional classical model, for the kinematically favored momenta for the two pulse durations. See text for details.

tunneling-ionization process. To this end, we plot in Figs. 6(a) and 6(b) the electric fields and the corresponding vector potentials for 4 fs and 8 fs laser pulses at a peak intensity of  $1.0 \times 10^{14} \text{ W/cm}^2$  with a wavelength of 790 nm and a CEP of 60°. According to the classical rescattering model, the first electron that escapes near  $t_1$  ( $t_2$ ) returns along the  $-\hat{z}$  ( $+\hat{z}$ ) direction to the parent ion around  $t_3$  ( $t_4$ ) when the vector potential is negative (positive). For a pulse duration of 4 fs, the absolute value of the electric field is smaller at  $t_1$  than at  $t_2$ and, therefore, the ionization probability of the first electron born near  $t_1$  is much smaller than that near  $t_2$ . This explains why the plateau of the right-side RWP, corresponding to the situation in which the first electron returns to the parent ion along the  $-\hat{z}$  direction, is about one order of magnitude lower than that of the left-side one, as demonstrated in Fig. 3(c). On the other hand, the difference between the left- and right-side RWPs for 8 fs (not shown) becomes much less pronounced since the (absolute) magnitudes of the electric field at  $t_1$  and  $t_2$  are closer to each other. While the tunneling ionization of the first electron associated with the RWP mainly affects the magnitude of the CMD, the tunneling ionization of the second electron plays an important role in shaping the CMD. Taking a CEP of  $\phi = 60^{\circ}$  as an example, one can see from Figs. 4 and 5 that, apart from the magnitude, the main change in the CMDs is that the momentum distribution along  $p_{\parallel}^2$  in the left-side CMD becomes wider as the pulse duration increases from 4 fs to 8 fs. As mentioned above, the momentum distribution along  $p_{\parallel}^2$  in the unsymmetrized CMD directly reflects the momentum distribution of the second tunnel-ionized electron.

Based on the one-dimensional (1D) classical model, if the initial velocity of the tunneling electron released at time t can be neglected, the final momentum of the second tunnelionized electron at the end of the pulse is given by

$$p_{\parallel}^2 = -\int_t^{\infty} F(t) dt = -A(t).$$
 (20)

The above equation indicates that the momentum of the tunneling electron is limited by  $-A_{+}^{\text{max}} \leq p_{\parallel}^{2} \leq A_{-}^{\text{max}}$ , where  $A_{+}^{\text{max}}$ and  $A_{-}^{\text{max}}$  are the extreme (absolute) values of the vector potential when it is positive and negative, respectively, during the time between recollision and the end of the pulse. For the return time  $t_3$  that is close to the center of the laser pulse, corresponding to the right-side momentum distribution, both  $A_{\perp}^{\text{max}}$  and  $A_{\perp}^{\text{max}}$  for 4 fs and 8 fs are close to  $A_0$ , where  $A_0$  is the maximum value of the vector potential, as shown in Fig. 6(b). This explains why the widths of the momentum distributions along  $p_{\parallel}^2$  in the right-side CMDs for 4 fs and 8 fs are close to each other. In contrast, for the return time  $t_4$ , corresponding to the left-side momentum distribution,  $A_{-}^{max}$  for 4 fs is almost two times smaller than that for 8 fs due to the envelope of the laser pulse. Explicitly, as marked by the arrows in Fig. 6(c),  $(-A_{\perp}^{\text{max}}, A_{\perp}^{\text{max}}) = (-0.75, 0.46)$  and (-0.87, 0.79) for 4 fs and 8 fs laser pulses, respectively.

It can be seen from Fig. 6(c) that the TDSE calculations, indeed, favor the 1D classical model, as also demonstrated in Refs. [27,40], where the 2D momentum spectra, from which the parallel momentum distributions of the tunnel-ionized electron were obtained, were presented. The above analysis clearly reveals that the width of the parallel momentum distribution for the second electron is completely determined by the maximum (positive and negative) values of the vector potential during the time of tunnel ionization that, in turn, is controlled by the temporal shape of the pulse. While the narrow parallel momentum distribution for the second tunnelionized electron and the corresponding RWP with a high plateau are responsible for the cross-shaped CMD for 4 fs laser pulses, the wide parallel momentum distribution for the second electron causes the collapse of the cross shape in the CMD for 8 fs laser pulses. It should be noted that the above discussion based on the situation for  $\phi = 60^{\circ}$  also applies to all other CEPs.

# D. Direct comparisons with experiments

With a full understanding of how the cross-shaped CMD is formed for 4 fs and why the cross shape collapses in the CMD for 8 fs, we next present direct comparisons of our model results with the experiments in which the CEP-averaged CMDs for pulse durations from 4 fs to 30 fs were measured. For the sake of completeness, we also calculated the CMDs for NSDI of Ar in 16 fs and 30 fs laser pulses with a wavelength of 790 nm at a peak intensity of  $1.0 \times 10^{14}$  W/cm<sup>2</sup>. The obtained results together with those for 4 fs and 8 fs are displayed and compared with the corresponding experimental measurements [17] in Fig. 7. Our theoretical results include the contributions of excitations of Ar<sup>+</sup> from the ground state to  $3s3p^6$ ,  $3s^23p^43d$ , and  $3s^23p^44s$ . The CEP-averaged CMDs

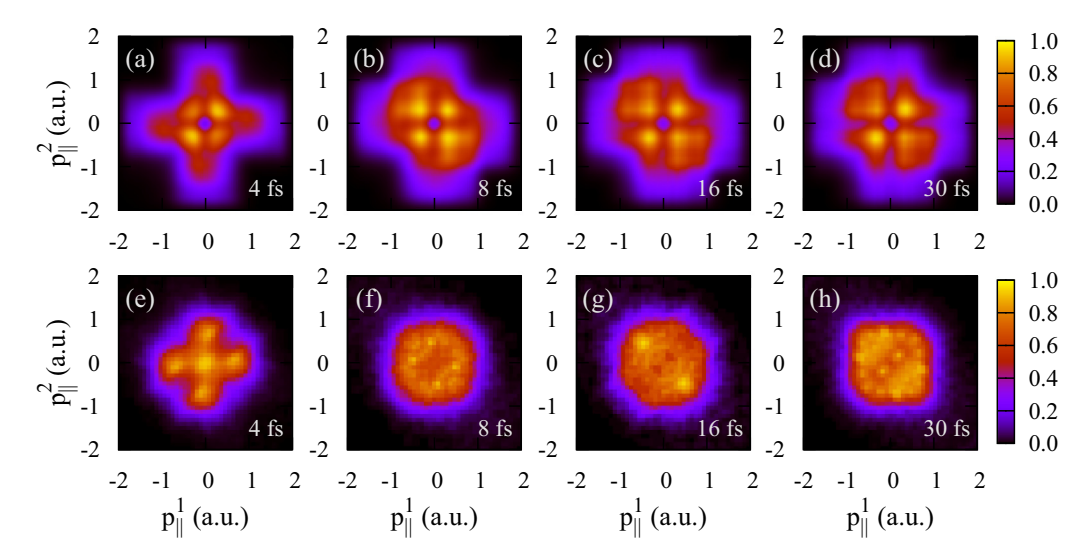


FIG. 7. Normalized correlated two-electron momentum distribution  $D(p_{\parallel}^1, p_{\parallel}^2)$  for NSDI of Ar in 790 nm laser pulses with a peak intensity of  $1.0 \times 10^{14}$  W/cm<sup>2</sup>. The theoretical results (top row) and the experimental measurements [17] (bottom row) are compared for pulse durations of 4 fs (a),(e), 8 fs (b),(f), 16 fs (a),(e), and 30 fs (a),(e), respectively. The results for 4 fs and 8 fs are CEP averaged. The theoretical results include the contributions of excitations of Ar<sup>+</sup> from the ground state to  $3s3p^6$ ,  $3s^23p^43d$ , and  $3s^23p^44s$ . See text for more details.

for 4 fs and 8 fs shown in Figs. 7(a) and 7(b) are only slightly different from those in Figs. 4(d) and 5(d) in which only the excitation to  $3s^23p^43d$  is considered, indicating that excitations to higher excited states can be safely neglected.

It can be seen from Fig. 7 that the QRS model well reproduces the overall pattern of the experimental findings. The main difference is that the computed CMDs predict significantly less double-ionization events with both electron momenta being close to zero. In addition, a slight suppression along the axes in the simulated CMDs visible even in Fig. 7(a) is not observed in the experiment. Both of the discrepancies are due to the kinematical constraint for the parallel momentum of the first rescattered electron [see Eq. (15) in Ref. [40]]. This indicates that some other mechanism, such as laser-induced decay of doubly excited states [35,41], which was not considered in the present QRS model, might be responsible for the discrepancies between the theoretical and experimental results.

Furthermore, in both theory and experiment, starting from a cross shape for 4 fs pulses, the signal is more homogeneously distributed over the four quadrants in the CMDs for the longer pulse durations, and the shapes of the CMDs for multicycle laser pulses (8 fs, 16 fs, and 30 fs) do not significantly differ from each other. However, a more careful examination reveals that, from 8 fs to 30 fs, the experimental CMDs exhibit a trend towards increasing anticorrelated electron emission (i.e., the momentum vectors of the two electrons point to opposing directions). This contradicts the predictions of the QRS model.

# IV. CONCLUSIONS AND OUTLOOK

Using the QRS model, we computed the CMDs for NSDI of Ar in 790 nm laser pulses at a peak intensity of  $1.0 \times 10^{14} \text{ W/cm}^2$  with pulse durations of 4 fs, 8 fs, 16 fs, and 30 fs, respectively. For the laser parameters considered here, we

only took into account recollision excitation with subsequent ionization of  $Ar^+$  in the excited states of  $3s3p^6$ ,  $3s^23p^43d$ , and  $3s^23p^44s$ . The differential cross sections for laser-free electron impact excitation of  $Ar^+$  were calculated with the R-matrix method, and the momentum distributions for electrons tunnel-ionized from the excited states of  $Ar^+$  were evaluated by solving the TDSE. The interferences between the excited pathways, the left and right distributions, and in the symmetrization due to the electron indistinguishability were not taken into account in the present work, although it is possible to consider these interferences with the QRS model.

In the present work, we focus on unveiling the mechanisms for the cross-shaped CMD for 4 fs and the collapse of the cross shape in the CMD for 8 fs. Our study reveals that the strong backward scattering of the first returning electron from the parent ion, due to the low incident energy (the maximum energy of the returning electron is less than 20 eV), and the narrow parallel momentum distribution (the maximum value of the parallel momentum is about half of  $A_0$ ) for the tunnel-ionized electron, owing to the restriction of the carrier envelope on the laser pulse, are responsible for forming the cross-shaped CMD (CEP averaged) for 4 fs. This mechanism is different from that for the cross shape observed in an earlier experiment [16] at a higher peak intensity of  $3.0 \times 10^{14} \text{ W/cm}^2$ ; see Ref. [23].

We further find that the collapse of the cross shape when the pulse duration is increased to 8 fs results from the significant change in the temporal shape of the laser pulse. Since the consecutive local field maxima near the center of the pulse at t=0 have almost the same absolute value for 8 fs laser pulses, no significant discrepancies exist between left-side and right-side recolliding wave packets, which are associated with tunnel ionization of the first electron returning to the parent ion along  $+\hat{z}$  and  $-\hat{z}$ , respectively. As a result, the magnitudes of the left-side and right-side CMDs are almost the same.

More importantly, due to the same reason, the widths of the momentum distributions along  $p_{\parallel}^2$  in the left-side and right-side CMDs also become comparative and are close to  $2A_0$ . The side arm for 4 fs then turns out to be approximately a square shape for 8 fs, leading to the collapse of the cross-shaped CMD.

Finally, the simulated CMDs are compared directly with the corresponding experimental measurements performed by Kübel *et al.* [17]. Our results are in qualitative agreement with the experimental findings for all pulse durations considered here. The main difference between theory and experiment is that the QRS model predicts significantly less double-ionization events with both electron momenta being close to zero. This implies that, apart from the laser-induced recollisional excitation tunneling, other mechanisms might be involved in the NSDI process for the experimental conditions considered here. It should also be noted that the subtle trend towards increasing anticorrelated electron emission in the CMDs for pulse durations between 8 fs and 30 fs observed experimentally was not reproduced by the QRS model either.

Consequently, further work on the effect of pulse duration on anticorrelation has been initiated.

#### ACKNOWLEDGMENTS

We are deeply indebted to our late colleague, Dr. O. Zatsarinny, who carried out the *B*-spline *R*-matrix calculations for electron-impact excitation of Ar<sup>+</sup>. We wish to thank Dr. M. Kübel for providing the experimental data plotted in Fig. 7 in digital form. This work was supported by the National Natural Science Foundation of China under Grant No. 11274219 and Guangdong Basic and Applied Basic Research Foundation, China, under Grant No. 2021A1515010047. T.M. was supported in part by the Japan Society for the Promotion of Science under Grants No. 19H00887 and No. 21K03417. K.B. was supported by the U.S. National Science Foundation under Grants No. PHY-1803844 and No. OAC-1834740, as well as the XSEDE Allocation No. PHY-090031. S.F. acknowledges funding by the Deutsche Forschungsgemeinschaft (DFG, German Research Foundation) under Project No. 440556973.

- A. L'Huillier, L. A. Lompre, G. Mainfray, and C. Manus, Phys. Rev. Lett. 48, 1814 (1982); Phys. Rev. A 27, 2503 (1983).
- [2] D. N. Fittinghoff, P. R. Bolton, B. Chang, and K. C. Kulander, Phys. Rev. Lett. 69, 2642 (1992).
- [3] B. Walker, E. Mevel, B. Yang, P. Breger, J. P. Chambaret, A. Antonetti, L. F. DiMauro, and P. Agostini, Phys. Rev. A 48, R894 (1993).
- [4] B. Walker, B. Sheehy, L. F. DiMauro, P. Agostini, K. J. Schafer, and K. C. Kulander, Phys. Rev. Lett. 73, 1227 (1994).
- [5] R. Lafon, J. L. Chaloupka, B. Sheehy, P. M. Paul, P. Agostini, K. C. Kulander, and L. F. DiMauro, Phys. Rev. Lett. 86, 2762 (2001).
- [6] B. Feuerstein, R. Moshammer, D. Fischer, A. Dorn, C. D. Schröter, J. Deipenwisch, J. R. Crespo Lopez-Urrutia, C. Höhr, P. Neumayer, J. Ullrich, H. Rottke, C. Trump, M. Wittmann, G. Korn, and W. Sandner, Phys. Rev. Lett. 87, 043003 (2001).
- [7] E. Eremina, X. Liu, H. Rottke, W. Sandner, A. Dreischuh, F. Lindner, F. Grasbon, G. G. Gaulus, H. Walther, R. Moshammer, B. Feuerstein, and J. Ullrich, J. Phys. B 36, 3269 (2003).
- [8] R. Moshammer, J. Ullrich, B. Feuerstein, D. Fischer, A. Dorn, C. D. Schröter, J. R. Crespo López-Urrutia, C. Höhr, H. Rottke, C. Trump, M. Wittmann, G. Korn, K. Hoffmann, and W. Sandner, J. Phys. B 36, L113 (2003).
- [9] Th. Weber, H. Giessen, M. Weckenbrock, G. Urbasch, A. Staudte, L. Spielberger, O. Jagutzki, V. Mergel, M. Vollmer, and R. Dörner, Nature (London) 405, 658 (2000).
- [10] M. Weckenbrock, D. Zeidler, A. Staudte, Th. Weber, M. Schöffler, M. Meckel, S. Kammer, M. Smolarski, O. Jagutzki, V. R. Bhardwaj, D. M. Rayner, D. M. Villeneuve, P. B. Corkum, and R. Dörner, Phys. Rev. Lett. 92, 213002 (2004).
- [11] A. Staudte, C. Ruiz, M. Schöffler, S. Schössler, D. Zeidler, Th. Weber, M. Meckel, D. M. Villeneuve, P. B. Corkum, A. Becker, and R. Dörner, Phys. Rev. Lett. 99, 263002 (2007).
- [12] A. Rudenko, V. L. B. de Jesus, Th. Ergler, K. Zrost, B. Feuerstein, C. D. Schröter, R. Moshammer, and J. Ullrich, Phys. Rev. Lett. 99, 263003 (2007).

- [13] Y. Liu, S. Tschuch, A. Rudenko, M. Dürr, M. Siegel, U. Morgner, R. Moshammer, and J. Ullrich, Phys. Rev. Lett. 101, 053001 (2008).
- [14] Y. Liu, D. Ye, J. Liu, A. Rudenko, S. Tschuch, M. Dürr, M. Siegel, U. Morgner, Q. Gong, R. Moshammer, and J. Ullrich, Phys. Rev. Lett. 104, 173002 (2010).
- [15] N. Camus, B. Fischer, M. Kremer, V. Sharma, A. Rudenko, B. Bergues, M. Kübel, N. G. Johnson, M. F. Kling, T. Pfeifer, J. Ullrich, and R. Moshammer, Phys. Rev. Lett. 108, 073003 (2012).
- [16] B. Bergues, M. Kübel, N. G. Johnson, B. Fischer, N. Camus, K. J. Betsch, O. Herrwerth, A. Senftleben, A. M. Sayler, T. Rathje, T. Pfeifer, I. Ben-Itzhak, R. R. Jones, G. G. Paulus, F. Krausz, R. Moshammer, J. Ullrich, and M. F. Kling, Nat. Commun. 3, 813 (2012).
- [17] M. Kübel, K. J. Betsch, N. G. Kling, A. S. Alnaserr, J. Schmidt, U. Kleineberg, Y. Deng, I. Ben-Itzhak, G. G. Paulus, T. Pfeifer, J. Ullrich, R. Moshammer, M. F. Kling, and B. Bergues, New J. Phys. 16, 033008 (2014).
- [18] A. S. Maxwell and C. Figueira de Morisson Faria, Phys. Rev. Lett. 116, 143001 (2016).
- [19] C. F. Faria, T. Shaaran, and M. T. Nygren, Phys. Rev. A 86, 053405 (2012).
- [20] C. Huang, Y. Zhou, Q. Zhang, and P. Lu, Opt. Express 21, 11382 (2013).
- [21] M. Kübel, C. Burger, N. G. Kling, T. Pischke, L. Beaufore, I. Ben-Itzhak, G. G. Paulus, J. Ullrich, T. Pfeifer, R. Moshammer, M. F. Kling, and B. Bergues, Phys. Rev. A 93, 053422 (2016).
- [22] A. Chen, M. Kübel, B. Bergues, M. F. Kling, and A. Emmanouilidou, Sci. Rep. 7, 7488 (2017).
- [23] Z. Chen, F. Liu, H. Wen, T. Morishita, O. Zatsarinny, and K. Bartschat, Opt. Express 28, 22231 (2020).
- [24] T. Morishita, A.-T. Le, Z. Chen, and C. D. Lin, Phys. Rev. Lett. 100, 013903 (2008).
- [25] T. Morishita and O. I. Tolstikhin, Phys. Rev. A 96, 053416 (2017).

- [26] Y. Chen, Y. Zhou, Y. Li, M. Li, P. Lan, and P. Lu, J. Chem. Phys. 144, 024304 (2016).
- [27] Z. Chen, Y. Wang, T. Morishita, X. Hao, J. Chen, O. Zatsarinny, and K. Bartschat, Phys. Rev. A 100, 023405 (2019).
- [28] P. B. Corkum, Phys. Rev. Lett. 71, 1994 (1993).
- [29] Z. Chen, A.-T. Le, T. Morishita, and C. D. Lin, Phys. Rev. A 79, 033409 (2009).
- [30] Z. Chen, T. Morishita, A.-T. Le, and C. D. Lin, Phys. Rev. A 76, 043402 (2007).
- [31] B. Böning, W. Paufler, and S. Fritzsche, Phys. Rev. A 99, 053404 (2019).
- [32] X. M. Tong and C. D. Lin, J. Phys. B 38, 2593 (2005).
- [33] Z. Chen, F. Liu, and H. Wen, Chin. Phys. B 28, 123401 (2019).
- [34] Z. Chen, Y. Liang, and C. D. Lin, Phys. Rev. Lett. 104, 253201 (2010).

- [35] Z. Chen, Y. Liang, and C. D. Lin, Phys. Rev. A 82, 063417 (2010).
- [36] O. Zatsarinny, Comput. Phys. Commun. 174, 273 (2006).
- [37] O. Zatsarinny and K. Bartschat, J. Phys. B 46, 112001 (2013).
- [38] H. W. van der Hart and K. Burnett, Phys. Rev. A 62, 013407 (2000).
- [39] T. Morishita, Z. Chen, S. Watanabe, and C. D. Lin, Phys. Rev. A **75**, 023407 (2007).
- [40] Z. Chen, A. Zhou, T. Morishita, Y. Bai, X. Hao, O. Zatsarinny, and K. Bartschat, Phys. Rev. A 103, 053102 (2021).
- [41] Y. Liu, L. Fu, D. Ye, J. Liu, M. Li, C. Wu, Q. Gong, R. Moshammer, and J. Ullrich, Phys. Rev. Lett. 112, 013003 (2014).